First and Second Order Mur Type ABCs for DNG Media

Ayşegül Pekmezci [1], Ercan Topuz [1], and Levent Sevgi [2]

[1] Department of Electronics and Communications Engineering
Dogus University, 34722 Kadikoy, Istanbul, Turkey
apekmezci@dogus.edu.tr, etopuz@dogus.edu.tr

[2] Department of Electrical and Electronics Engineering
Okan University, 34959 Tuzla, Istanbul, Turkey
levent.sevgi@okan.edu.tr

Abstract ─ Reflections from boundaries of the FDTD computational domain lead to inaccurate, even unstable codes when dealing with problems involving double negative (DNG) materials. Here, an efficient and simple algorithm is presented for terminating FDTD in DNG medium which is based on first and second order Mur's absorbing boundary conditions (ABC). FDTD update equations for Mur's ABC formulations are obtained from frequency domain one-way wave equations using piecewise linear recursive convolution (PLRC) method. Numerical examples are given both for 1D and 2D scenarios to demonstrate the validity and stability of the proposed Mur formulations, and its advantages over uniaxial perfectly matched layer (UPML) in reducing computational time and memory requirements.

Index Terms ─ Absorbing Boundary Conditions (ABC), Double Negative Media (DNG), Finite Difference Time Domain (FDTD), Lorentz model, MUR, one-way wave equation.

I. INTRODUCTION

FDTD formulation is a convenient tool for solution of electromagnetic wave problems. Often it becomes necessary to terminate computational domain at fictitious boundaries which ideally absorb all incident radiation without producing any reflection. The most widely used ABCs are Mur [1], perfectly matched layer (PML) [2-5] types and the recently proposed surface impedance ABCs [6,7]. Although PML performance is significantly better than Mur's ABC particularly when dealing with a wider range of incident angles, Mur's ABC may be preferred due to its computational efficiency and ease of implementation whenever the level of reflections can be tolerated.

In the presence of DNG medium special care is required in implementing Mur or PML ABCs to ensure stability. In literature, one can find several studies on the use of PML in DNG media [8-11]. Kosmas et al. presented an ABC based on Mur's approach using dispersive media with a single pole conductivity z-transform model [12]. In this study, a novel formulation of first and second order Mur's ABC has been developed for truncating the DNG media for 1D and 2D problems using PLRC-FDTD algorithm [13]. In the following sections, formulation of the proposed method is presented and its validity and stability as well as its computational advantages over UPML is demonstrated via numerical examples considering a domain filled entirely with Lorentz type DNG material.

It should be noted two factors limit the applicability domain of the formulation presented in this paper. The first one is the assumption of identical dispersion models for electric and magnetic susceptibilities to enable the Fourier transform of the refractive index $n(\omega) = \sqrt{\varepsilon_r(\omega)\mu_r(\omega)}$ to be performed analytically. The second one is the approximation of the square root terms in the one-way split-operator form of the wave equation in 2nd order Mur formulation by two term Taylor series expansion. Thereby introduced limitations are discussed in the following sections.

II. NUMERICAL METHOD

A. Formulation of first-order DNG-Mur ABC

In linear, isotropic, and homogenous DNG media the wave equation becomes:

$$\nabla^2 E(\omega) + k^2(\omega) E(\omega) = 0; \; k(\omega) = \frac{\omega}{c} n(\omega), \quad (1)$$

where E is a field component, $k(\omega)$ is the wave number and c is free space wave velocity. The frequency dependent refractive index $n(\omega)$ is written as:

$$n(\omega) = \sqrt{\varepsilon_r(\omega)\mu_r(\omega)} = \sqrt{[1+\chi_e(\omega)][1+\chi_m(\omega)]}. \quad (2)$$

In numerical calculations single pole Lorentz model is used for electric and magnetic susceptibilities, $\chi_e(\omega), \chi_m(\omega)$ as in [14]:

$$\chi_{e,m}(\omega) = \frac{\omega_{pe,pm}^2}{\omega_{oe,om}^2 - \omega^2 + j\Gamma_{e,m}\omega}, \qquad (3)$$

where $\omega_{pe,pm}$ is the plasma frequency, $\omega_{oe,om}$ is the resonance frequency, and $\Gamma_{e,m}$ is the damping coefficient, respectively. Considering a 1D case, where $\partial/\partial y \equiv \partial/\partial z \equiv 0$, right and left going waves can be separated as:

$$\left(\frac{\partial^2}{\partial x^2} + \frac{\omega^2}{c^2} n(\omega)^2\right) E(\omega) = \left(\frac{\partial}{\partial x} + \frac{j\omega}{c} n(\omega)\right)$$
$$\cdot \left(\frac{\partial}{\partial x} - \frac{j\omega}{c} n(\omega)\right) E(\omega) = 0 \qquad (4)$$

The functional form of (2) complicates inverse Fourier transform of the operators in (4). A convenient way of avoiding this complication is to approximate geometric mean in (2) by its arithmetic mean. This approach is found to be rather effective when source spectrum is centered close to the intersection point of the $\chi_e(\omega)$ and $\chi_m(\omega)$. However, for purposes of brevity, in this letter we present the formulations for the case of identical models for $\varepsilon_r(\omega)$ and $\mu_r(\omega)$ to write the refractive index as $n(\omega) = 1 + \chi_e(\omega)$. Then the left going waves in (4) yields:

$$\frac{\partial E(\omega)}{\partial x} - \frac{j\omega}{c} E(\omega) - \frac{j\omega}{c} P(\omega) = 0, \qquad (5)$$

$$P(\omega) = \chi_e(\omega) E(\omega) . \qquad (6)$$

Inverse Fourier transform of (5-6) yields:

$$\frac{\partial E(t)}{\partial x} - \frac{1}{c}\frac{\partial E(t)}{\partial t} - \frac{1}{c}\frac{\partial P(t)}{\partial t} = 0, \qquad (7)$$

$$P(t) = \chi_e(t) * E(t), \qquad (8)$$

where '*' denotes convolution in time domain and electric susceptibility function in time domain $\chi_e(t)$ is obtained from (3) as:

$$\chi_e(t) = \gamma_e e^{-\alpha_e t} \sin(\beta_e t) u(t), \qquad (9)$$

where $\alpha_e = \Gamma_e/2$, $\beta_e = \sqrt{\omega_{oe}^2 - \Gamma_e^2/4}$ and $\gamma_e = \omega_{pe}^2/\beta_e$. To derive an FDTD update equation for implementing one-way absorbing boundary condition, (7) is discretized using two-point centered difference approximation at mesh point i+1/2 and at time index n+1/2:

$$E\big|_i^{n+1} = E\big|_{i+1}^n + \left(\frac{c\Delta t - \Delta x}{c\Delta t + \Delta x}\right)\left[E\big|_{i+1}^{n+1} - E\big|_i^n\right]$$
$$- \left(\frac{\Delta x}{c\Delta t + \Delta x}\right)\left[P\big|_{i+1}^{n+1} - P\big|_{i+1}^n + P\big|_i^{n+1} - P\big|_i^n\right] \qquad .(10)$$

Here, i and n are the indices of discrete space and time variables, Δx and Δt are spatial and temporal discretization step sizes, respectively. The discrete form

of P^n is obtained by using PLRC method [13] where the multiplication in frequency domain corresponds to the convolution integral in time domain and discretized as a running sum. Imposing causality, the convolution term in (8) can be defined as:

$$P(t) = \chi_e(t) * E(t) = \int_0^t E(t-\tau)\chi_e(\tau)d\tau . \qquad (11)$$

The discretized convolution integral is then obtained by inserting $t = n\Delta t$ into (11):

$$P\big|_i^n = \int_0^{n\Delta t} E(n\Delta t - \tau)\chi_e(\tau)d\tau \bigg|_i . \qquad (12)$$

Approximating the variation of E fields with a linear function in successive Δt interval $q\Delta t \le \tau \le (q+1)\Delta t$, one can write:

$$E(n\Delta t - \tau) = E^{n-q} + \frac{E^{n-q-1} - E^{n-q}}{\Delta t}(\tau - q\Delta t). \qquad (13)$$

Substitution of (13) into (12) yields:

$$P\big|_i^n = \sum_{q=0}^{n-1}\int_{q\Delta t}^{(q+1)\Delta t}\left[E^{n-q} + \frac{E^{n-q-1} - E^{n-q}}{\Delta t}(\tau - q\Delta t)\right]\chi_e(\tau)d\tau \bigg|_i ,$$
$$= \sum_{q=0}^{n-1}\left\{E\big|_i^{n-q}\chi_e^q + \left(E\big|_i^{n-q-1} - E\big|_i^{n-q}\right)\xi_e^q\right\}$$
$$\qquad (14)$$

where

$$\chi_e^q = \int_{q\Delta t}^{(q+1)\Delta t}\chi_e(\tau)d\tau , \qquad (15a)$$

$$\xi_e^q = \frac{1}{\Delta t}\int_{q\Delta t}^{(q+1)\Delta t}(\tau - q\Delta t)\chi_e(\tau)d\tau , \qquad (15b)$$

which can be evaluated using (9) and following the steps given in [13,14]. The P terms in the right side of (10) can then be expressed as:

$$P\big|_{i+1}^{n+1} - P\big|_{i+1}^n + P\big|_i^{n+1} - P\big|_i^n = \xi_e^0\left[E\big|_{i+1}^n + E\big|_i^n\right]$$
$$+ \left(\chi_e^0 - \xi_e^0\right)\left[E\big|_{i+1}^{n+1} + E\big|_i^{n+1}\right] - \psi_e\big|_{i+1}^n - \psi_e\big|_i^n \qquad , (16)$$

where ψ_e^n is known as the recursive accumulator and given by:

$$\psi_e\big|_i^n = \sum_{q=0}^{n-1}\left[\left(\Delta\chi_e^q - \Delta\xi_e^q\right)E\big|_i^{n-q} + \Delta\xi_e^q E\big|_i^{n-q-1}\right], \qquad (17a)$$

with

$$\Delta\chi_e^q = \chi_e^q - \chi_e^{q+1} \; ; \; \Delta\xi_e^q = \xi_e^q - \xi_e^{q+1}. \qquad (17b)$$

Substituting (16) into (10) and rearranging the discrete equation, one obtains FDTD update equations for left (i=1) and right (i=K) side boundaries:

$$E\big|_1^{n+1} = a_1 E\big|_2^{n+1} + a_2 E\big|_2^n - a_3 E\big|_1^n + a_4\left[\psi_e\big|_2^n + \psi_e\big|_1^n\right]$$
$$E\big|_K^{n+1} = a_1 E\big|_{K-1}^{n+1} + a_2 E\big|_{K-1}^n - a_3 E\big|_K^n + a_4\left[\psi_e\big|_{K-1}^n + \psi_e\big|_K^n\right] \qquad , (18)$$

with

$$c_1 = \left(\frac{c\Delta t - \Delta x}{c\Delta t + \Delta x}\right); c_2 = \left(\frac{\Delta x}{c\Delta t + \Delta x}\right); c_3 = \left(\chi_e^0 - \xi_e^0\right); c_4 = \xi_e^0;$$

$$a_1 = \left(\frac{c_1 - c_2 c_3}{1 + c_2 c_3}\right); a_2 = \left(\frac{1 - c_2 c_4}{1 + c_2 c_3}\right); a_3 = \left(\frac{c_1 + c_2 c_4}{1 + c_2 c_3}\right); a_4 = \left(\frac{c_2}{1 + c_2 c_3}\right)$$

B. Formulation of second-order DNG-Mur ABC

The first-order DNG-Mur's boundary is suitable for 1D problem, where the wave is propagating normal to boundaries. In more general problems, wave propagates toward boundaries at an arbitrary angle. In those cases, obviously, 2nd order approximation is superior to the 1st order approximation in reducing reflections from boundaries of the computational domain. Considering 2D case $\left(\partial/\partial z \equiv 0\right)$ where only the E_z field components impinge on the left and right boundaries along x-direction (i.e., on x=0 and x=h), the wave equation is factored as in the following:

$$\left(\frac{\partial^2}{\partial x^2} + \frac{\partial^2}{\partial y^2} + \frac{\omega^2}{c^2}n(\omega)^2\right)E(\omega) = \left(D_x^2 + D_y^2 - D_\omega^2 n(\omega)^2\right)E(\omega)$$

$$= \left(D_x + D_\omega n(\omega)\sqrt{1 - S_x^2}\right)\left(D_x - D_\omega n(\omega)\sqrt{1 - S_x^2}\right)E(\omega) = 0$$

(19)

where

$$S_x^2 = \frac{D_y^2}{n(\omega)^2 D_\omega^2}, \qquad (20a)$$

$$D_x \equiv \frac{\partial}{\partial x}, D_y^2 \equiv \frac{\partial^2}{\partial y^2}, D_\omega \equiv \frac{j\omega}{c}, D_\omega^2 \equiv -\frac{\omega^2}{c^2}. \qquad (20b)$$

Approximating the square root term with a two-term Taylor series expansion as $\sqrt{1 - S_x^2} \cong 1 - S_x^2/2$ and substituting S_x^2 and $n(\omega)$ into (19) one can write the one-way wave equation which satisfies the backward wave condition along x-direction as:

$$\left(D_x - D_\omega n(\omega)\left(1 - \frac{S_x^2}{2}\right)\right)E(\omega)$$

$$= j\omega \frac{\partial E(\omega)}{\partial x} + \frac{\omega^2}{c}E(\omega) + \frac{\omega^2}{c}P(\omega) + \frac{c}{2}R(\omega) = 0$$

(21)

where

$$P(\omega) = \chi_e(\omega)E(\omega)$$

$$R(\omega) = \frac{\partial^2 E(\omega)}{\partial y^2} - Q(\omega). \qquad (22)$$

$$Q(\omega) = R(\omega)\chi_e(\omega)$$

Taking the inverse Fourier transform of (21) yields:

$$c\frac{\partial^2 E(t)}{\partial t \partial x} - \frac{\partial^2 E(t)}{\partial t^2} - \frac{\partial^2 P(t)}{\partial t^2} + \frac{c^2}{2}R(t) = 0, \quad (23)$$

where

$$P(t) = \chi_e(t) * E(t)$$

$$R(t) = \frac{\partial^2 E(t)}{\partial y^2} - Q(t). \qquad (24)$$

$$Q(t) = \chi_e(t) * R(t)$$

Similar to 1D formulation, discrete forms of P, Q and R are obtained using PLRC algorithm:

$$P\big|_{(i,j)}^{n+1} = \left\{2P^n - P^{n-1} + p_1 E^{n+1} + p_2 E^n + p_3 E^{n-1} + \psi_e^n\right\}\big|_{(i,j)}$$

$$Q\big|_{(i,j)}^{n+1} = \left\{Q^n + p_1 R^{n+1} + \xi_e^0 R^n - \phi_e^n\right\}\big|_{(i,j)}$$

$$R\big|_{(i,j)}^{n+1} = \left[\frac{E\big|_{(i,j+1)}^{n+1} - 2E\big|_{(i,j)}^{n+1} + E\big|_{(i,j-1)}^{n+1}}{\Delta y^2}\right] - Q\big|_{(i,j)}^{n+1}$$

(25)

Here, ψ_e^n and ϕ_e^n are known as the recursive accumulator and given by:

$$\psi_e^n(i,j) = \sum_{q=0}^{n-2}\left[\begin{array}{c}\left(\Delta\chi_e^q - \Delta\xi_e^q\right)E^{n-q-1}(i,j) \\ + \Delta\xi_e^q E^{n-q-2}(i,j)\end{array}\right], \quad (26a)$$

$$\phi_e^n(i,j) = \sum_{q=0}^{n-1}\left[\begin{array}{c}\left(\Delta\chi_{ee}^q - \Delta\xi_{ee}^q\right)R^{n-q}(i,j) \\ + \Delta\xi_{ee}^q R^{n-q-1}(i,j)\end{array}\right], \quad (26b)$$

where

$$\Delta\chi_e^q = \chi_e^{q+2} - 2\chi_e^{q+1} + \chi_e^q; \Delta\chi_{ee}^q = \chi_e^q - \chi_e^{q+1}, \quad (27a)$$

$$\Delta\xi_e^q = \xi_e^{q+2} - 2\xi_e^{q+1} + \xi_e^q; \Delta\xi_{ee}^q = \xi_e^q - \xi_e^{q+1}. \quad (27b)$$

Using central-difference expressions for the space and time derivatives in (23) and substituting discrete form of P, Q and R from (25) one obtains:

$$E\big|_{(1,j)}^{n+1} = e_1 E\big|_{(2,j)}^{n+1} + e_2 E\big|_{(2,j)}^n + e_3 E\big|_{(1,j)}^n - e_4 E\big|_{(2,j)}^{n-1}$$

$$+ e_5 E\big|_{(1,j)}^{n-1} - e_6\left[\psi_e\big|_{(2,j)}^n + \psi_e\big|_{(1,j)}^n\right] \qquad , \quad (28)$$

$$+ e_7\left[R\big|_{(2,j)}^n + R\big|_{(1,j)}^n\right]$$

with

$$p_1 = \left(\chi_e^0 - \xi_e^0\right); p_2 = \left(\chi_e^1 - \xi_e^1 - 2\chi_e^0 + 3\xi_e^0\right); p_3 = \left(\xi_e^1 - 2\xi_e^0\right)$$

$$e_0 = \frac{c\Delta t/\Delta x + 1 + p_1}{2\Delta t^2}; e_1 = \frac{c\Delta t/\Delta x - 1 - p_1}{2\Delta t^2 e_0}; e_2 = e_3 = \frac{2 - p_2}{2\Delta t^2 e_0};$$

$$e_4 = \frac{c\Delta t/\Delta x + 1 + p_3}{2\Delta t^2 e_0}; e_5 = \frac{c\Delta t/\Delta x - 1 - p_3}{2\Delta t^2 e_0}; e_6 = \frac{1}{2\Delta t^2 e_0}; e_7 = \frac{c^2}{4e_0}.$$

Analogous FDTD expressions for the 2nd order DNG-Mur ABC on the other boundaries can be derived in the same manner.

III. NUMERICAL RESULTS

In this section, first numerical results are presented both for 1D and 2D cases where the problem space is filled entirely with DNG medium modelled by identical Lorentz parameters for $\varepsilon_r(\omega), \mu_r(\omega)$ and boundaries on both sides are terminated with proposed DNG-Mur ABCs. In all simulations, a tapered sinusoidal pulse (5-10-5 pulse described in [15]) is used as excitation with a center frequency of $f_s = 7.5$ GHz, and inserted at the center of the FDTD grid. The Lorentz type medium parameters are chosen as $\omega_{pe} = \omega_{pm} = \omega_s\sqrt{48/25}$, $\omega_{oe} = \omega_{om} = \omega_s/5$ and $\Gamma_e = \Gamma_m = \omega_s/200$, which yields

a refractive index about -1 at the center frequency $\left(\omega_s = 2\pi f_s\right)$. FDTD grid parameters are $\Delta x = 0.067\,\text{cm}$ for 1D case and $\Delta x = \Delta y = 0.2\,\text{cm}$ for 2D case with a time step of 0.5 times the Courant limit. Total FDTD domain is chosen as 1000 grid and 400x400 grid for 1D and 2D scenarios, respectively.

Absorbing performance of the proposed formulations are illustrated via reflections from the DNG-Mur boundaries. The reflection coefficient at an observation point is determined by calculating the test and reference field strength versus time using proposed FDTD formulations in two steps [10]. In the first step, the test field E_{test} is calculated at an observation point 2-cells away from the DNG-Mur boundary. In the second step, incident field E_{inc} is obtained by repeating the same calculations, but now considering a larger domain so that boundary reflected fields cannot reach the observation point during the time window of step one. The reflected field can then be obtained as $E_{\text{ref}}(t) = E_{\text{test}}(t) - E_{\text{inc}}(t)$. Then, the reflection coefficient at each frequency is calculated by dividing the discrete Fourier transforms (DFT) of reflected field and incident fields.

In Fig. 1, frequency spectrum of the incident field is shown together with reflection coefficients obtained using DNG-Mur ABCs in 1D and 2D scenarios. For comparison purposes the reflection coefficients obtained using 10-cell thick DNG-UPML ABCs are also plotted. The computation time and memory requirements for both approaches are listed in Table 1. Our numerical results show that 1D and 2D DNG-Mur ABCs reduce reflections to about -60dB and -50dB level over the 7.1−7.9 GHz band under the main lobe and require less memory and computational time than DNG-UPML simulations.
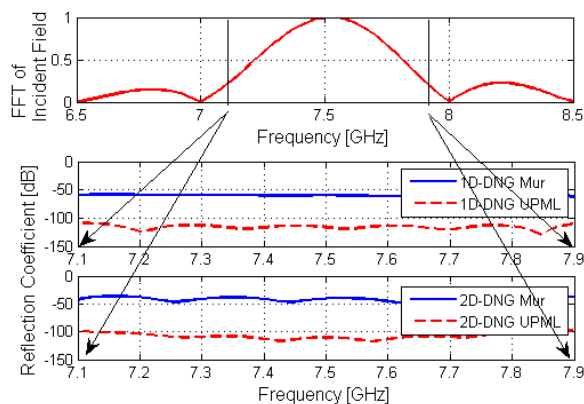
Fig. 1. Frequency spectrum of incident field, and reflection coefficients both for DNG-Mur and DNG-UPML for 1D and 2D scenarios.

We have also calculated the reflection coefficients performance of proposed DNG-Mur ABCs for the case

of non-identical Lorentz models using arithmetic mean approach outlined in Sec. IIA. The results obtained with the same parameters for $\chi_e(\omega)$, but $\omega_{pm} = \omega_s$, $\omega_{om} = \omega_s/\sqrt{2}$ and $\Gamma_m = \omega_s/200$ for $\chi_m(\omega)$ are found to differ less than ± 3 dB from those shown in Fig. 1, over the entire frequency range.
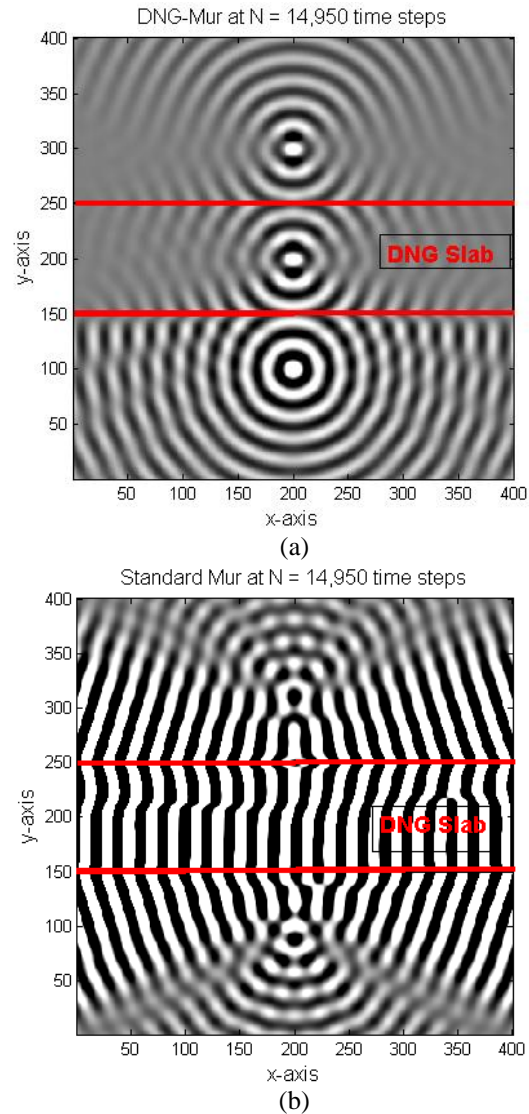
Fig. 2. Snapshot of propagation through DNG slab using: (a) DNG-Mur and (b) standard Mur.

As a second 2D test we consider a DNG slab with a thickness along y-direction about $100\Delta y$ imbedded in air, extending infinitely in x, z, and excited by a z-directed line source. We have used 50-1000-50 cycle [15] source at $f_s = 7.5$ GHz. This yields near-perfect match conditions as steady-state conditions set up, and the refractive index of the slab approaches to -1 (-0.9999-

0.0104j). In order to demonstrate the effectiveness of the proposed extension of Mur formalism to DNG media we performed two simulation runs, one using DNG-Mur and the other using Standard-Mur at slab boundaries. For the first simulation, boundaries of the 400x400 grid size computational domain are terminated with standard 2D Mur ABC for air, and with 2D DNG-Mur ABC for the DNG slab boundaries at y-grid points between 150 and 250 (See Fig. 2 (a)). For the second simulation, standard 2D Mur ABC is used at all boundaries (both air and DNG slab, See Fig. 2 (b)). The line source is placed at a point where x=200Δx, y=100Δy, i.e., at a distance 50Δy from the DNG slab for both simulations, and typical outputs are depicted in Fig. 2 (a), Fig. 3 (a), and Fig. 2 (b), Fig. 3 (b), respectively.

(a)

(b)
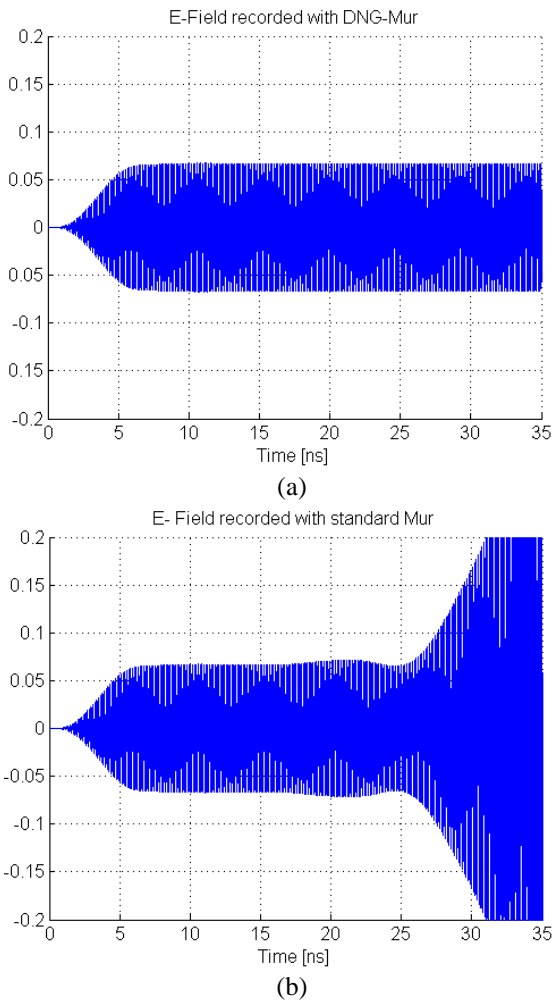
Fig. 3. Time domain field recorded at an observation point while DNG slab is truncated with a) DNG-Mur and b) Standard Mur.

The snapshot given in Fig. 2 (a) clearly shows the cylindrical wave fronts emanating from the source, as well as from the anticipated image locations [15,16] inside and behind the slab. In Fig. 3 (a) the time history of the E field at an observation point located between source and slab is given which demonstrates the stability of the code when terminating slab boundaries with DNG-Mur. Figure 2 (b) and Fig. 3 (b) correspond to similar outputs obtained when, at slab boundaries, DNG-Mur is replaced with standard Mur. Figure 2 (b) and Fig. 3 (b) show that reflections from improperly terminated boundaries of the DNG slab results in instability after about 10,000 time steps, and completely corrupts field distribution inside the computational domain by 14,950 steps, as shown in Fig. 2 (b).

Table 1: Memory usage and computation time in FDTD simulations for DNG-Mur and DNG-UPML ABCs

FDTD Grid		Time (s)	Memory (MB)
2D Case 1000x1000 cells t=5000Δt	Mur	1693.9	244.45
	UPML	3881.5	516.98
1D Case 1000 cells t=10000Δt	Mur	1.73	0.72
	UPML	2.65	0.87

IV. CONCLUSION

Absorbing boundary conditions based on Mur's approach have been developed for DNG media in 1D and 2D FDTD computational domain. In the presented formulations, DNG slab is modeled with identical Lorentz parameters for $\varepsilon_r(\omega), \mu_r(\omega)$ in frequency dependent one-way wave equations and PLRC method is used to derive FDTD update equations. 1D and 2D simulations demonstrate that the proposed implementations of Mur ABC for terminating DNG media provide stable results and effectively reduce boundary reflections by about 50 dB, which may be acceptable in many applications. Comparison of computational requirements for DNG-Mur and DNG-UPML as listed in Table 1 indicate that the DNG-Mur provides definite advantages both in memory and computation time. The formulations given in this paper are valid for any dispersive media and can be also applied for Drude model.

REFERENCES

[1]   G. Mur, "Absorbing boundary conditions for the finite difference approximation of the time-domain electromagnetic-field equations," *IEEE Trans. Electromagn. Compat.*, vol. 23, no. 4, pp.377-382, 1981.

[2]   J. P. Berenger, "Three-dimensional perfectly matched layer for the absorption of electromagnetic waves," *J. Computat. Phys.*, vol. 127, pp. 363-379, 1996.

[3]   S. D. Gedney, "An anisotropic perfectly matched layer-absorbing medium for the truncation of

FDTD lattices," *IEEE Trans. Antennas Propag.*, vol. 44, pp. 1630-1639, Dec. 1996.

[4] M. Kuzuoglu and R. Mittra, "Frequency dependence of the constitutive parameters of causal perfectly matched anisotropic absorbers," *IEEE Microw. Guided Wave Lett.*, vol. 6, pp. 447-449, 1996.

[5] J. Roden and S. D. Gedney, "Convolution PML (CPML): An efficient FDTD implementation of the CFS-PML for arbitrary media," *Microw. Opt. Technol. Lett.*, vol. 27, pp. 334-339, 2000.

[6] Y. Mao, A. Z. Elsherbeni, S. Li, and T. Jiang, "Surface impedance absorbing boundary for terminating FDTD simulations," *ACES Journal*, vol. 29, no. 12, pp. 1035-1046, 2014.

[7] Y. Mao, A. Z. Elsherbeni, S. Li, and T. Jiang, "Non-uniform surface impedance absorbing boundary condition for FDTD method," *ACES Express Journal*, vol. 1, no. 7, pp. 197-200, July 2016.

[8] S. D. Gedney, "An anisotropic PML absorbing media for the FDTD simulation of fields in lossy and dispersive media," *Electromagnetics*, vol. 16, no. 4, pp. 399-415, 1996.

[9] S. A. Cummer, "Perfectly matched layer behavior in negative refractive index materials," *IEEE Antennas Wireless Propagat. Lett.*, vol. 3, pp. 172-175, 2004.

[10] K. Zheng, W.-Y. Tam, D.-B. Ge, and J.-D. Xu, "Uniaxial PML absorbing boundary condition for truncating the boundary of DNG metamaterials," *PIERL*, vol. 8, 125-134, 2009.

[11] D. Correia and J. M Jin, "3D-FDTD-PML analysis of left-handed metamaterials," *Microw. Opt. Technol. Lett.*, vol. 40, no. 3, pp. 201-205, Feb. 2004.

[12] P. Kosmas and C. Rappaport, "A simple absorbing boundary condition for FDTD modeling of lossy, dispersive media based on the one-way wave equation," *IEEE Trans. Antennas Propagat.*, vol. 52, no. 9, pp. 2476-2479, Sept. 2004.

[13] D. Kelley and R. J. Luebbers, "Piecewise linear recursive convolution for dispersive media using FDTD," *IEEE Trans. Antennas Propagat.*, vol. 44, no. 6, pp. 792-797, 1996.

[14] A. Pekmezci and L. Sevgi, "FDTD-based meta-material (MTM) modeling and simulation," *IEEE Antennas and Propagat. Magazine*, vol. 56, no. 5, pp. 289-303, Oct. 2014.

[15] R. W. Ziolkowski and E. Heyman, "Wave propagation in media having negative permittivity and permeability," *Phys. Rev. E*, vol. 64, 056625, 2001.

[16] J. B. Pendry, "Negative refraction makes a perfect lens," *Physical Review Letters*, vol. 85, no. 18, pp. 3966-3969, Oct. 2000.
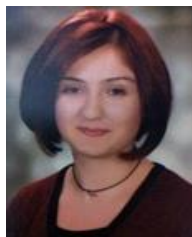
Aysegul Pekmezci was born in Zonguldak, Turkey, in February 1984. She received a B.S. and an M.S. degree in Electrical and Electronics Engineering from University of Gaziantep, Gaziantep, Turkey in 2007 and 2010. Currently, she is with the Department of Electronics and Communications Engineering, Dogus University at Istanbul, Turkey and pursuing her Ph.D. studies in Institute of Science and Technology of the same university. Her research interests are primarily in the analytical and numerical solutions of electromagnetic wave problems, computational aspects of scattering and interaction with dispersive media.

Ercan Topuz received the M.S. and Ph.D. degrees in Electronics and Communication from Istanbul Technical University, Istanbul, Turkey, in 1965 and 1973, respectively. Currently, he is with the Department of Electronics and Communications Engineering, Dogus University at Istanbul, Turkey. He has authored or co-authored over 70 technical papers in books, journals, and conferences. His research interests include theoretical and computational electromagnetics, microwave/optical devices and systems. Topuz is a Member of the Electromagnetics Academy.

Levent Sevgi has been with Okan University since September 2014. He graduated from Istanbul Technical University (ITU) and completed his Ph.D studies with Prof. Leopold B. Felsen at Weber Research Institute/ New York Polytechnic University. His research study has focused on analytical and numerical methods in electromagnetics. He has published over 170 journal/magazine papers/tutorials and attended nearly 120 international conferences/ symposiums. His two books Complex Electromagnetic Problems and Numerical Simulation Approaches and Electromagnetic Modeling and Simulation were published by the IEEE Press - Wiley in 2003 and 2014, respectively.